Electronic Supplementary Information

Experimental Section

Materials: Sodium hydroxide (NaOH), ammonium chloride (NH_4Cl), potassium sulfate (K_2SO_4), hydrochloric acid (HCl), salicylic acid ($C_7H_6O_3$), sodium citrate dehydrate ($C_6H_5Na_3O_7·2H_2O$), *p*-dimethylaminobenzaldehyde ($C_9H_{11}NO$), Nafion solution (5 wt %), anhydrous alcohol, sodium nitroferricyanide dihydrate ($C_5FeN_6Na_2O·2H_2O$), sodium nitrite ($NaNO_2$) and sodium hypochlorite (NaClO) were purchased from Aladdin Ltd. (Shanghai, China). Nitric acid (HNO_3), sulfuric acid (H_2SO_4), hydrogen peroxide (H_2O_2), hydrazine monohydrate ($N_2H_4·H_2O$), phosphoric acid (H_3PO_4) and ethyl alcohol (C_2H_5OH) were purchased from Beijing Chemical Corp. (China). chemical Ltd. in Chengdu. Titanium plate (0.2 mm thick) was purchased from Qingyuan Metal Materials Co., Ltd (Xingtai, China). All reagents used in this work were analytical grade without further purification.

Synthesis of TiO_{2-x} NBA/TP: The fabrication process of TiO_{2-x} NBA/TP were as follows: Firstly, titanium plates were cut into small pieces (2.0 × 4.0 cm^2) and sonicated in acetone, ethanol, and distilled water for 15 min, respectively. After then, they were put into 40 mL of 5 M NaOH aqueous solution in 50 mL Teflon-lined autoclave. The autoclave was kept in an electric oven at 180℃ for 24 h. After the autoclave was cooled down naturally to room temperature, the samples were moved out, washed with deionized water and ethanol several times and dried at 60 ℃ for 30 min. Then the samples were immersed in 1 M HCl for 1 h in order to exchange Na^+ with H^+. The as-prepared $H_2Ti_2O_5·H_2O$ NBA/TP were rinsed with deionized water and ethanol several times and dried at 60 ℃ for 30 min. Subsequently, $H_2Ti_2O_5·H_2O$ NBA/TP were annealed in a tubular furnace at 500 ℃ for 2 h. After cooling to room temperature, TiO_{2-x} NBA/TP were finally obtained.

Preparation of the TiO_2/TP: Typically, 10 mg of the commercial TiO_2 nanoparticle powder and 10μL of Nafion solution (5 wt %) were scattered in a mixture of 500μL water and 500μL anhydrous alcohol by ultrasonic treatment for 1 h to form a homogeneous liquid. Then, 50μL of the dispersion was loaded on a TP with an area of 1 × 0.5 cm^2 and dried in the N_2 atmosphere at 60 °C for 1 h.

Characterizations: XRD data were acquired by a LabX XRD-6100 X-ray diffractometer with a Cu Kα radiation (40 kV, 30 mA) of wavelength 0.154 nm (SHIMADZU, Japan). SEM measurements were carried out on a Gemini SEM 300 scanning electron microscope (ZEISS, Germany) at an accelerating voltage of 5 kV. XPS measurements were performed on an ESCALABMK II X-ray

photoelectron spectrometer using Mg as the exciting source. The absorbance data of spectrophotometer were measured on UV-Vis spectrophotometer. TEM image was obtained from a Zeiss Libra 200FE transmission electron microscope operated at 200 kV. EPR spectrum was recorded on a Brüker EMX spectrometer at room temperature.

Electrochemical measurements: All electrochemical measurements were carried on the CHI660E electrochemical workstation (Shanghai, Chenhua) using a standard three-electrode setup. Electrolyte solution was Ar-saturated of 0.1 M NaOH with 0.1 M NO_2^-, using TiO_{2-x} NBA/TP (1.0 × 0.5 cm^2) as the working electrode, graphite rod as the counter electrode and a Hg/HgO as the reference electrode. We use a H-type electrolytic cell separated by a Nafion 117 membrane which was protonated by boiling in ultrapure water, H_2O_2 (5%) aqueous solution and 0.5 M H_2SO_4 at 80 °C for another 2 h, respectively. All the potentials reported in our work were converted to reversible hydrogen electrode via calibration with the following equation: E (RHE) = E (Hg/HgO) + (0.098 + 0.0591 × pH) V and the presented current density was normalized to the geometric surface area.

Determination of NH_3: The NH_3 concentration in the solution was determined by colorimetry (the obtained electrolyte was diluted 40 times) using the indophenol blue method.[1] In detail, 2 mL of the solution after reaction, and 2 mL of 1 M NaOH chromogenic solution containing 5% salicylic acid and 5% sodium citrate. Then, 1 mL oxidizing solution of 0.05 M NaClO and 0.2 mL catalyst solution of $C_5FeN_6Na_2O$ (1 wt%) were added to the above solution. After standing in the dark for 2 h, the UV-Vis absorption spectra were measured. The concentration of NH_3 was identified using the absorbance at a wavelength of 655 nm. The concentration-absorbance curve was calibrated using the standard NH_4Cl solution with NH_3 concentrations of 0.25, 0.50, 0.75, 1.0, 1.50, 2.50, 3.50 and 5.0 ppm in 0.1 M NaOH solution. The fitting curve ($y = 0.3896\ x + 0.0178$, $R^2 = 0.9996$) shows good linear relation of absorbance value with NH_3 concentration.

Determination of N_2H_4: In this work, we used the method of Watt and Chrisp to estimate whether N_2H_4 produced.[2] The chromogenic reagent was a mixed solution of 5.99 g $C_9H_{11}NO$, 30 mL HCl and 300 mL C_2H_5OH. In detail, 1 mL electrolyte was added into 1 mL prepared color reagent and standing for 15 min in the dark. The absorbance at 455 nm was measured to quantify the N_2H_4 concentration with a standard curve of hydrazine ($y = 0.6497\ x + 0.07655$, $R^2 = 0.9995$).

Calculations of the FE and NH_3 yield rate:

FE toward NH_3 via NO_2RR was calculated by the following equation (the reduction of NO_2^- to

NH_3 consumes six electrons):

$$FE = (6 \times F \times [NH_3] \times V) / (M_{NH3} \times Q) \times 100\% \quad (1)$$

NH_3 yield rate was calculated using the following equation:

$$NH_3 \text{ yield rate} = ([NH_3] \times V) / (M_{NH3} \times t \times A) \quad (2)$$

Where F is the Faradic constant (96500 C mol^{-1}), $[NH_3]$ is the measured NH_3 concentration, V is the volume of electrolyte in the cathode compartment (70 mL), M_{NH3} is the molar mass of NH_3, Q is the total quantity of applied electricity; t is the electrolysis time and A is the loaded area of catalyst (1.0×0.5 cm^2).

DFT calculation details:

First-principles calculations with spin-polarized were carried out based on density functional theory (DFT) implemented in the VASP package,[3] and the interaction between valence electrons and ionic core were expanded using the projector augmented wave (PAW) approach with a cutoff of 450 eV.[4] Perdew-Burke-Ernzerhof functional (PBE) with semi-empirical corrections of DFT-D3 was adopted to describe exchange-correlation functional effect based on general gradient approximation (GGA).[5] TiO_2(101) surface was modeled using a 2 × 2 supercell with three trilayers (O-Ti-O), of which the bottom trilayer was fixed. The thickness of the vacuum region is > 15 Å to avoid the spurious interaction. Hubbard U model was implemented with an effective U = 4 eV for Ti 3d orbitals.[6,7] The Brillouin zone was sampled by 2 × 3 × 1 special k-points using the Monkhorst Pack scheme for structural configuration optimizations.[8] The force convergence thresholds are 0.02 eV/Å and the total energy less than 1E-5 eV, respectively. The theoretical calculation results were processing and analyzed by VASPKIT software.[9]

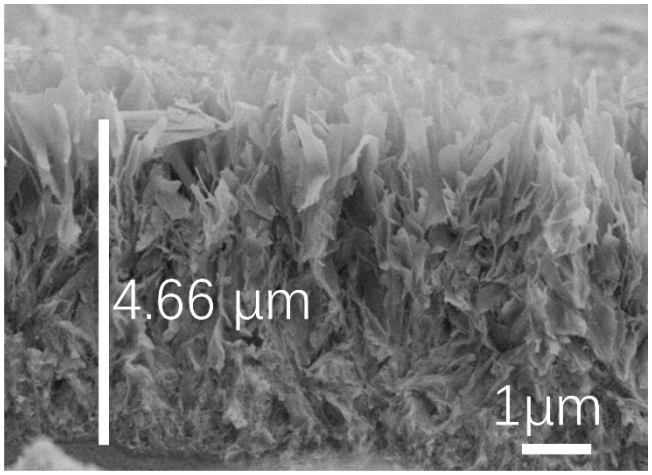

Fig. S1 Cross-section SEM image of TiO_{2-x} NBA/TP.

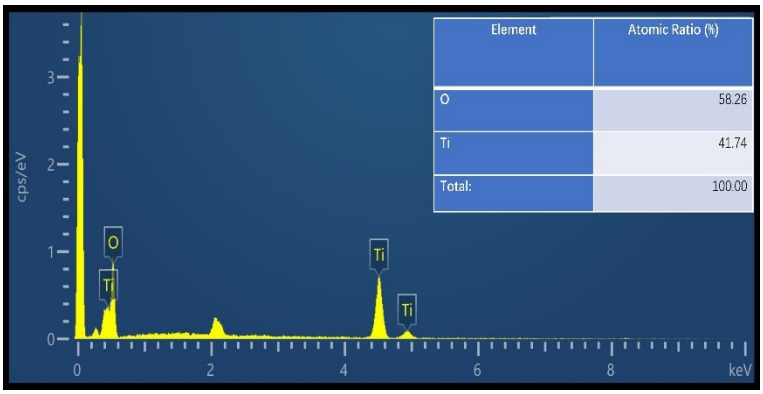

Fig. S2 The ratio of Ti and O of TiO_{2-x} NBA/TP.

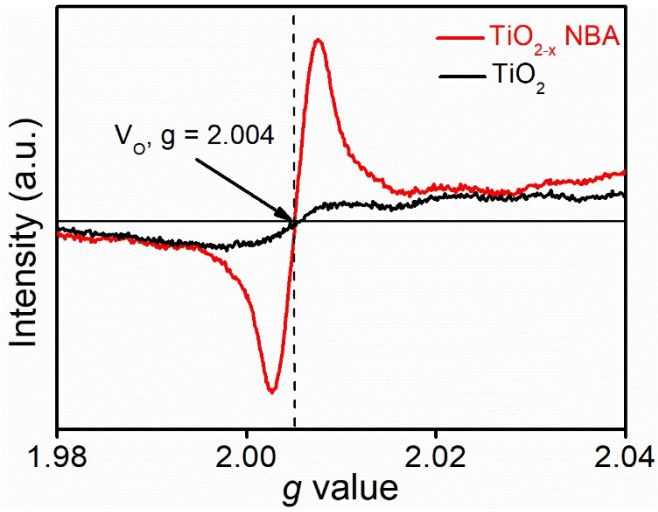

Fig. S3 EPR spectra of the commercial TiO_2 (black curve) and the TiO_{2-x} NBA (red curve).

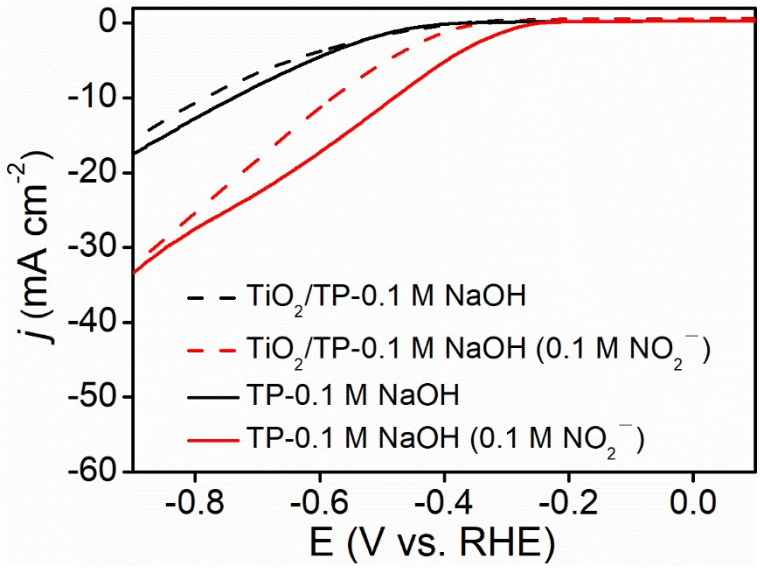

Fig. S4 LSV curves of TiO_2/TP and bare TP in 0.1 M NaOH with and without 0.1 M NO_2^-.

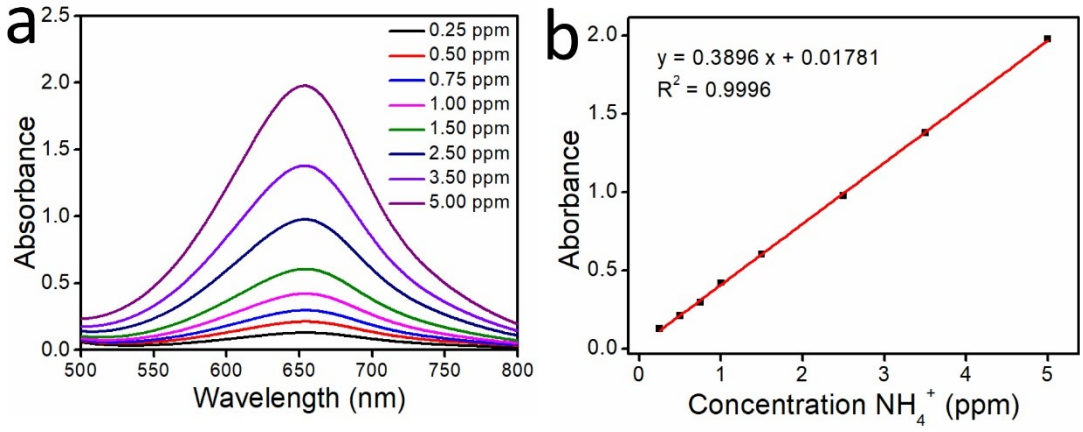

Fig. S5 (a) UV-Vis absorption spectra and corresponding (b) calibration curve used for calculation of NH_3 concentration.

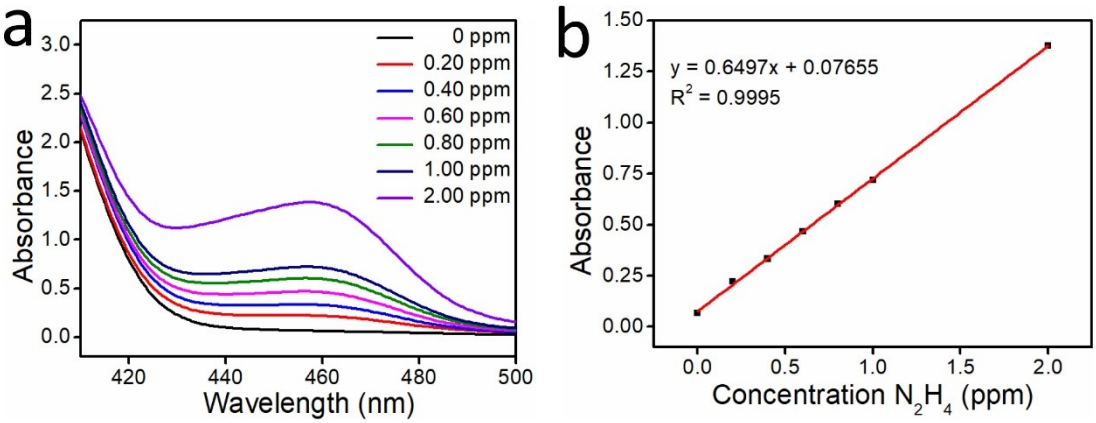

Fig. S6 (a) UV-Vis absorption spectra and corresponding (b) calibration curve used for calculation of N_2H_4 concentration.

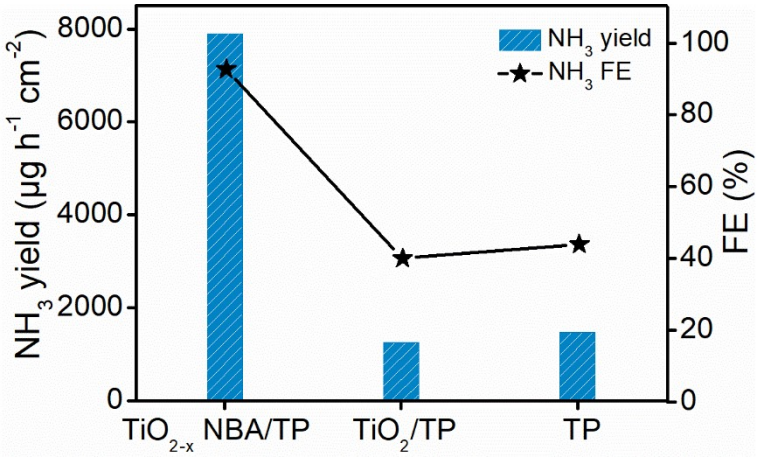

Fig. S7 Calculated NH_3 yields and FEs of TiO_{2-x} NBA/TP, TiO_2/TP and bare TP toward NO_2RR in 0.1 M NaOH with 0.1 M NO_2^- at −0.7 V.

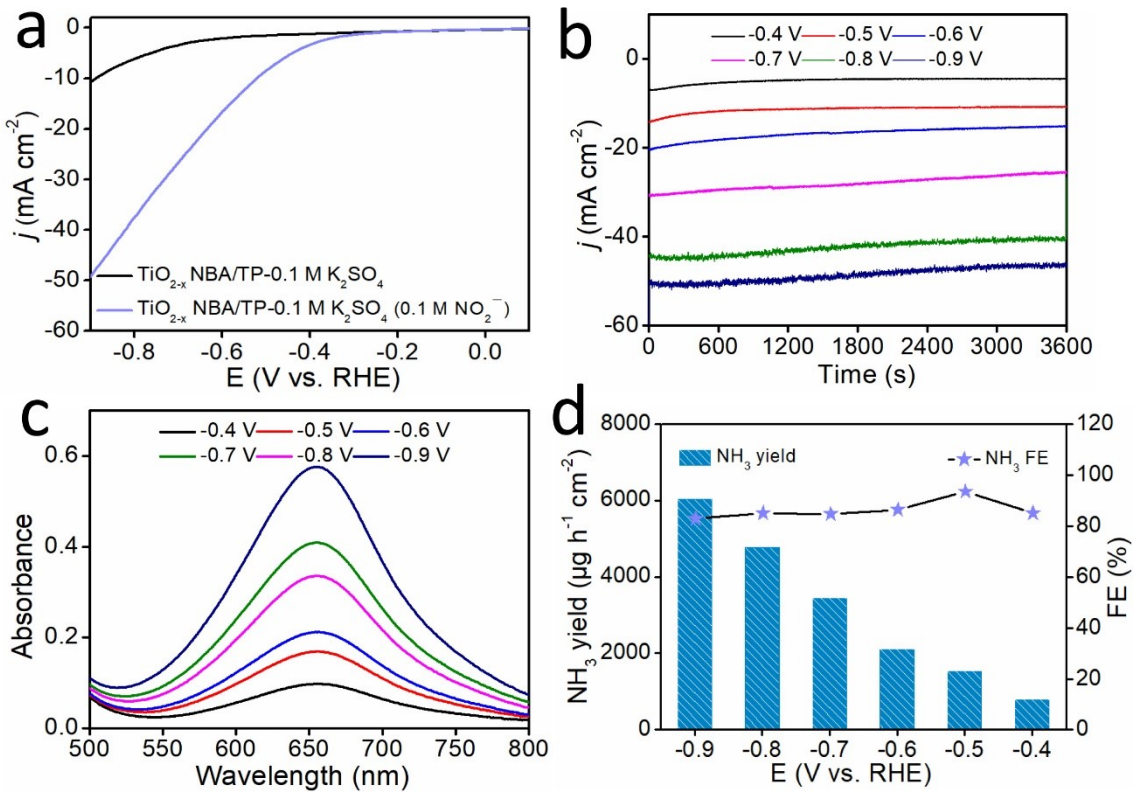

Fig. S8 (a) LSV curves of TiO_{2-x} NBA/TP in 0.1 M K_2SO_4 in the presence and absence of 0.1 M NO_2^-. (b) CA curves (from −0.4 V to −0.9 V) and (c) corresponding UV-Vis spectra of TiO_{2-x} NBA/TP. (d) Calculated NH_3 yields and FEs of TiO_{2-x} NBA/TP at different given potentials.

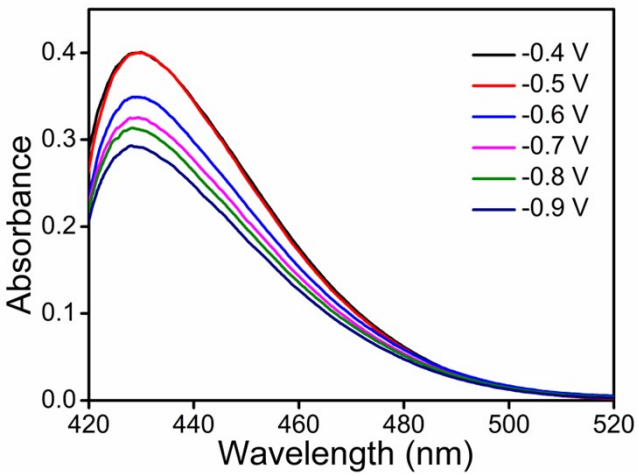

Fig. S9 UV-Vis absorption spectra of the electrolytes estimated by the method of Watt and Chrisp for the calculation of N_2H_4 concentration.

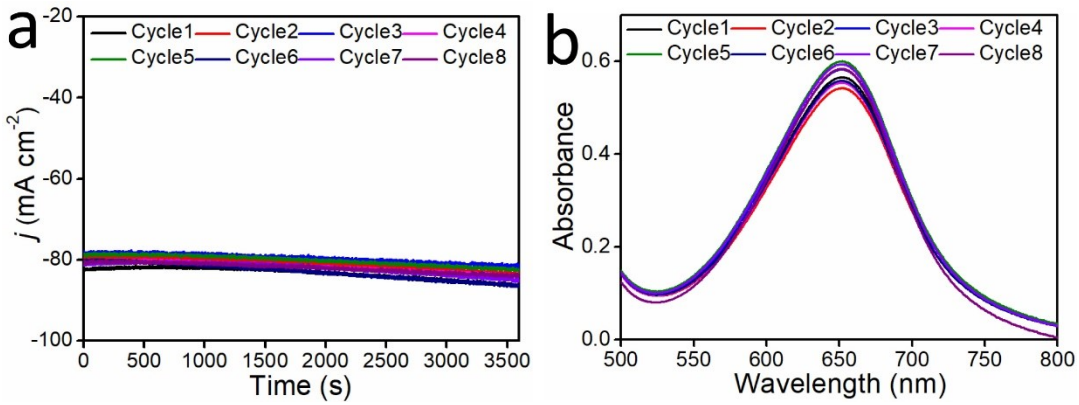

Fig. S10 (a) Chronoamperometry curves and (b) corresponding UV-Vis absorption spectra of TiO_{2-x} NBA/TP for electrochemical catalytic production of NH_3 during cycling tests in 0.1 M NaOH with 0.1 M NO_2^- at −0.7 V.

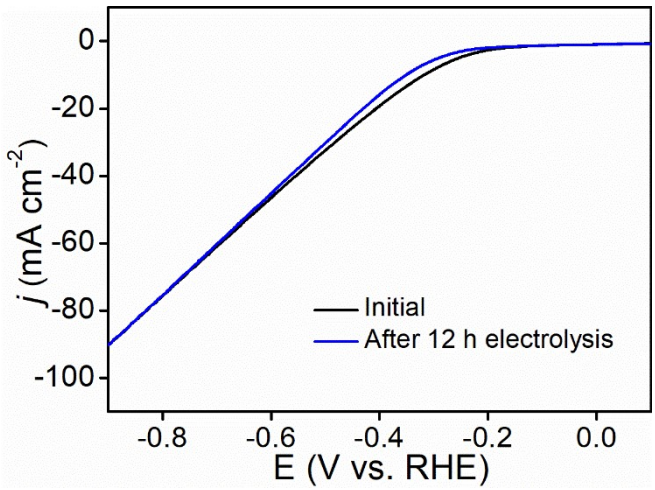

Fig. S11 LSV curves of TiO_{2-x} NBA/TP before and after 12 h electrolysis in 0.1 M NaOH with 0.1 M NO_2^-.

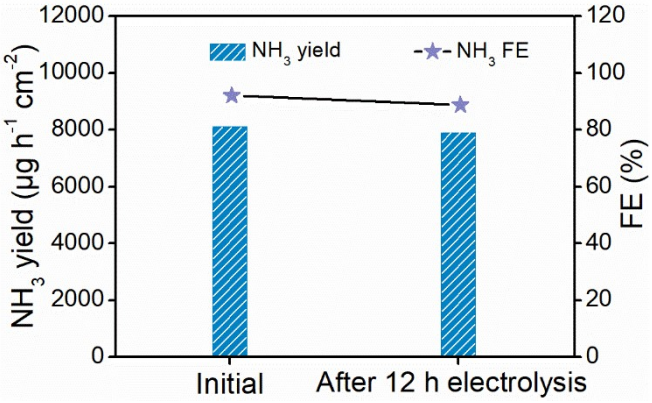

Fig. S12 NH_3 yields and FEs for TiO_{2-x} NBA/TP before and after 12 h electrolysis in 0.1 M NaOH with 0.1 M NO_2^- at −0.7 V.

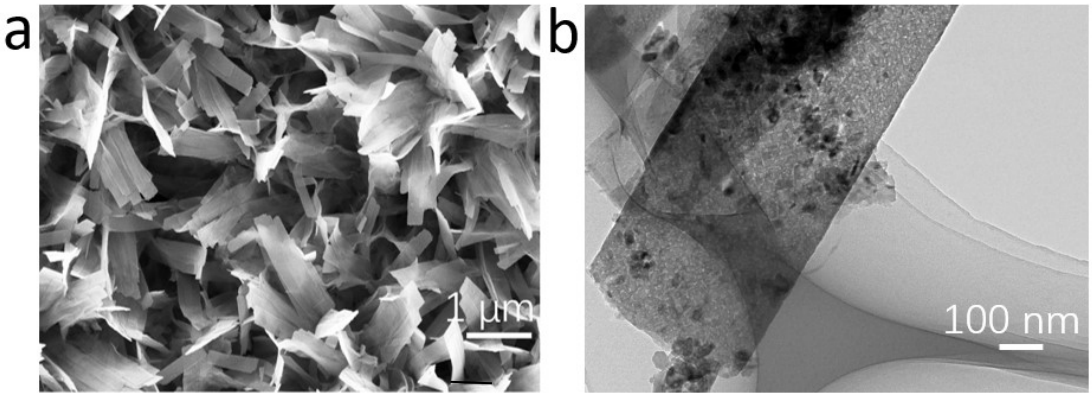

Fig. S13 (a) SEM and (b)TEM images for TiO_{2-x} NBA after 12 h electrolysis.

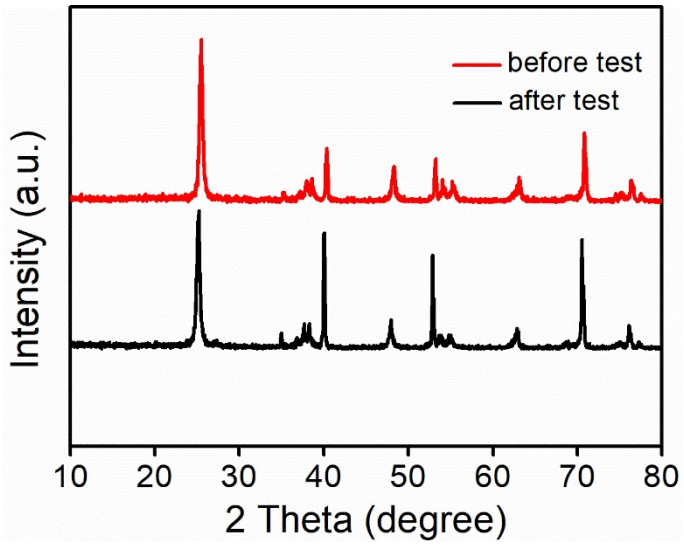

Fig. S14 XRD patterns for TiO_{2-x} NBA/TP.

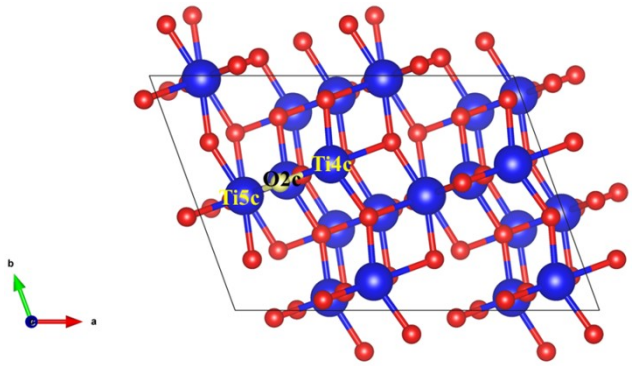

Fig. S15 Top views of TiO_2 (101) slab model with V_O.

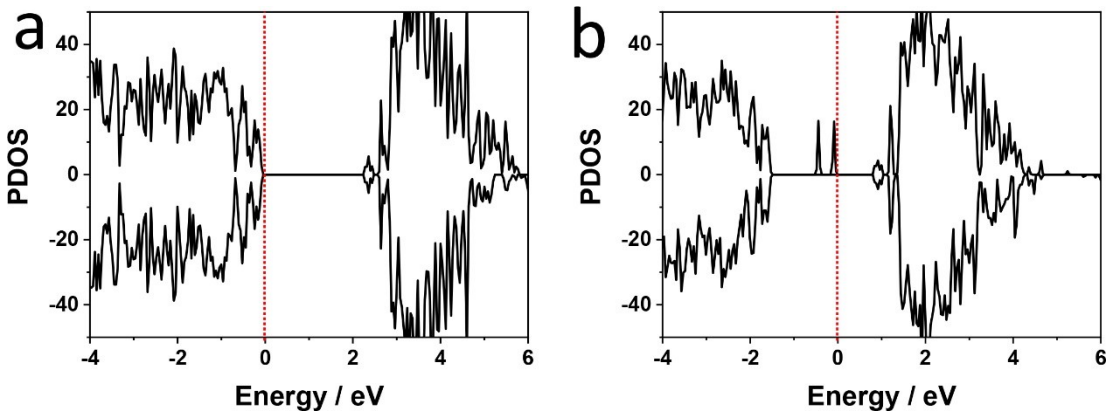

Fig. S16 DOS for TiO_2 (101) slab model without and with V_O.

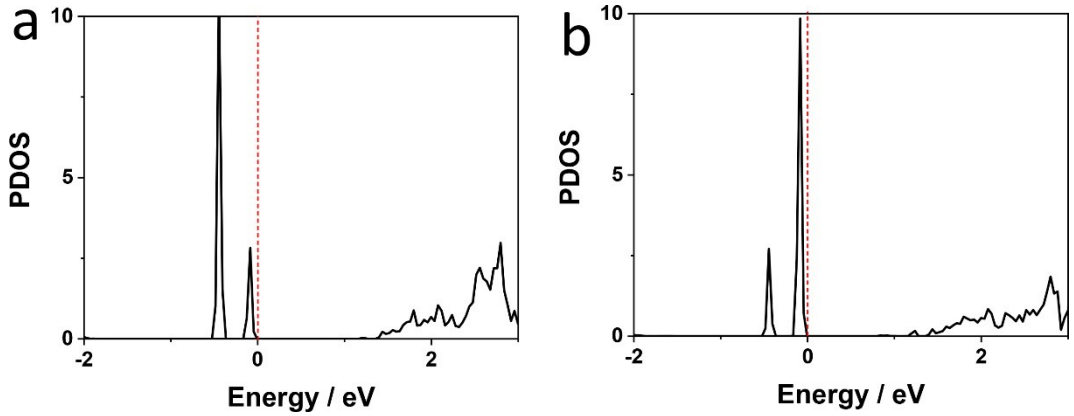

Fig. S17 DOS for Ti_{5c}^{3+} and Ti_{4c}^{3+} atoms induced by O_{2c} V_O, respectively.

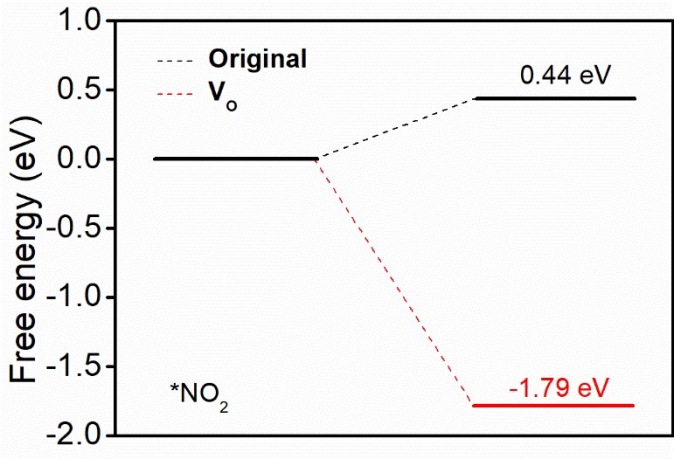

Fig. S18 Calculated free energies for NO_2^- adsorption on TiO_2 (101) slab model without and with V_O and corresponding atomic configurations.

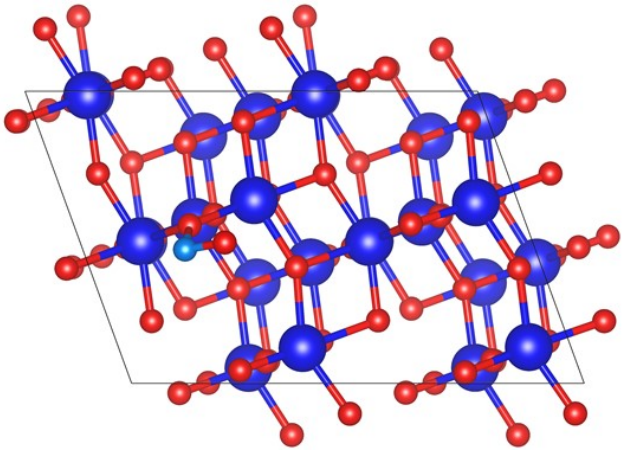

Fig. S19 Top views of NO_2^- adsorption on TiO_2 (101) surface with V_O.

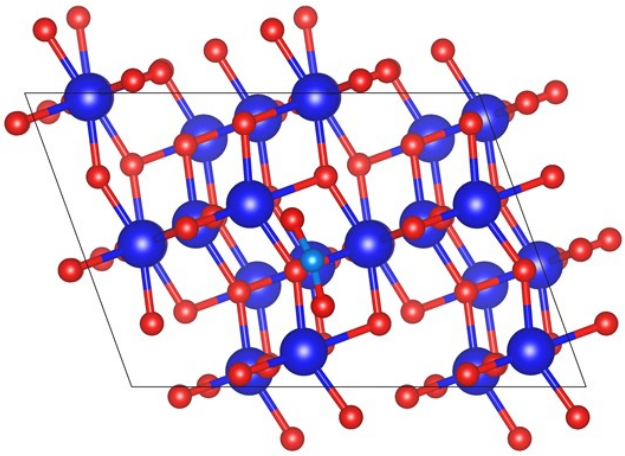

Fig. S20 Top views of NO_2^- adsorption on pristine TiO_2 (101) surface.

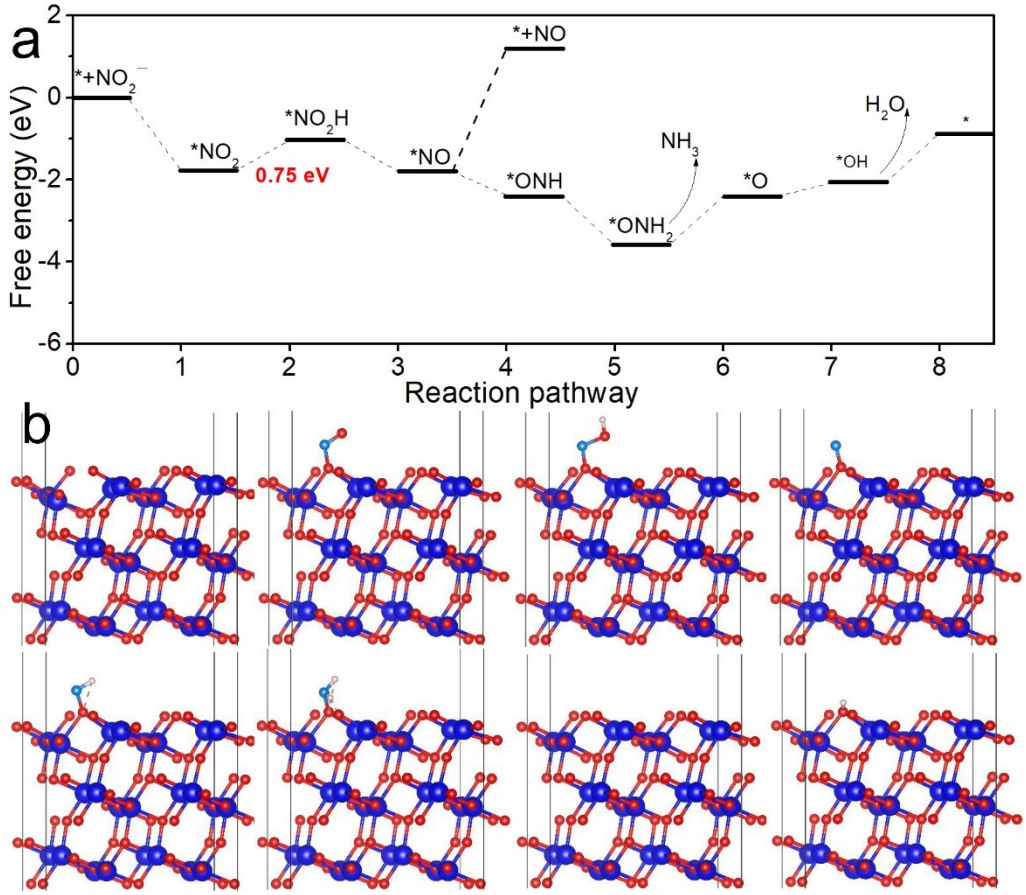

Fig. S21 (a) Free energy diagram of different intermediates generated during the NO_2RR on TiO_{2-x} (101) along with the optimal pathway and (b) corresponding atomic configurations.

Table S1 Comparison of the catalytic performances of TiO_{2-x} NBA/TP with other reported NO_2RR electrocatalysts under ambient conditions.

Catalyst	Electrolyte	Performance	Ref.
TiO_{2-x} NBA/TP	0.1 M NaOH ($NaNO_2$)	NH_3 yield rate: 7898 μg h^{-1} cm^{-2}, FE_{NH3}: 92.7%	This work
MnO_2 nanoarrays	0.1 M Na_2SO_4 ($NaNO_2$)	NH_3 yield rate: 3.09 × 10^{-11} mol s^{-1} cm^{-2}, FE_{NH3}: 6%	10
Cobalt-tripeptide complex	1.0 M MOPS (1.0 M $NaNO_2$)	NH_3 yield rate: 3.01 × 10^{-10} mol s^{-1} cm^{-2}, FE_{NH3}: 90 ± 3%	11
Poly-NiTRP complex	0.1 M $NaClO_4$ ($NaNO_2$)	NH_3 yield rate: 1.1 mM	12
Cu phthalocyanine complexes	0.1 M KOH ($NaNO_2$)	FE_{NH3}: 78%	13
$[Co(DIM)Br_2]^+$ (Carbon rod working electrode)	0.1 M solution of $NaNO_2$	FE_{NH3}: 88%	14
$Cu_{80}Ni_{20}$	1.0 M NaOH (20 mM $NaNO_2$)	FE_{NH3}: 87.6%	15
Cu_3P nanowire array	0.1 M PBS (0.1M $NaNO_2$)	NH_3 yield rate: 1626.6 ± 36.1 μg h^{-1} cm^{-2}, FE_{NH3}: 91.2 ± 2.5%	16
CoP nanoarray	0.1 M PBS (500 ppm $NaNO_2$)	NH_3 yield rate: 2260.7 ± 51.5 μg h^{-1} cm^{-2}, FE_{NH3}: 90 ± 2.3%	17
Ni_2P nanosheet array	0.1 M PBS (200 ppm $NaNO_2$)	NH_3 yield rate: 2692.2 ± 92.1 μg h^{-1} cm^{-2}, FE_{NH3}: 90.2 ± 3%	18
Oxo-MoS_x	0.1 M $NaNO_2$ in 0.2 M citric acid (pH = 5)	FE_{NH3}: 13.5%	19

Table S2 Standard electrode potentials for nitrite redox reactions.

Chemical reaction equation	Standard electrode potential
$2\ NO_2^- + 8\ H^+ + 6\ e^- \longleftrightarrow N_2\ (g) + 4\ H_2O$	$E^0 = 1.520$ V (vs. NHE)
$2\ NO_2^- + 2\ H^+ + e^- \longleftrightarrow NO\ (g) + H_2O$	$E^0 = 1.202$ V (vs. NHE)
$2\ NO_2^- + 6\ H^+ + 4\ e^- \longleftrightarrow N_2O\ (g) + 3\ H_2O$	$E^0 = 1.396$ V (vs. NHE)
$2\ NO_2^- + 6\ H^+ + 4\ e^- \longleftrightarrow NH_3OH^+ + H_2O$	$E^0 = 0.673$ V (vs. NHE)
$2\ NO_2^- + 8\ H^+ + 6\ e^- \longleftrightarrow NH_4^+ + 2\ H_2O$	$E^0 = 0.897$ V (vs. NHE)
$2\ NO_2^- \longleftrightarrow NO_2 + e^-$	$E^0 = 0.780$ V (vs. NHE)

References

1 D. Zhu, L. Zhang, R. E. Ruther and R. J. Hamers, *Nat. Mater*., 2013, **12**, 836–841.

2 G. W. Watt and J. D. Chrisp, *Anal. Chem*., 1952, **24**, 2006–2008.

3 G. Kresse and J. Hafner, *Phys. Rev. B*, 1994, **49**, 14251–14269.

4 G. Kresse and D. Joubert, *Phys. Rev. B*, 1999, **59**, 1758–1775.

5 J. P. Perdew, K. Burke and M. Ernzerhof, *Phys. Rev. Lett*., 1996, **77**, 3865–3868.

6 E. Finazzi, C. D. Valentin, G. Pacchioni and A. Selloni, *J. Chem. Phys*., 2008, **129**, 154113.

7 M. M. Islam, M. Calatayud and G. Pacchioni, *J. Phys. Chem. C*, 2011, **115**, 6809–6814.

8 H. J. Monkhorst and J. D. Pack, *Phys. Rev. B*, 1976, **13**, 5188–5192.

9 V. Wang, N. Xu, J. Liu, G. Tang and W. Geng, *Comput. Phys. Commun.*, 2021, **267**, 108033.

10 R. Wang, Z. Wang, X. Xiang, R. Zhang, X. Shi and X. Sun, *Chem. Commun*., 2018, **54**, 10340–10342.

11 Y. Guo, J. R. Stroka, B. Kandemir, C. E. Dickerson and K. L. Bren, *J. Am. Chem. Soc*., 2018, **140**, 16888–16892.

12 P. Dreyse, M. Isaacs, K. Calfumán, C. Cáceres, A. Aliaga, M. J. Aguirre and D. Villagra, *Electrochim. Acta*, 2011, **56**, 5230–5237.

13 N. Chebotareva and T. Nyokong, *J. Appl. Electrochem*., 1997, **27**, 975–981.

14 S. Xu, H. Y. Kwon, D. C. Ashley, C. H. Chen, E. Jakubikova and J. M. Smith, *Inorg. Chem*., 2019, **58**, 9443–9451.

15 L. Mattarozzi, S. Cattarin, N. Comisso, P. Guerriero, M. Musiani, L. V. Gómez and E. Verlato, *Electrochim. Acta*, 2013, **89**, 488–496.

16 J. Liang, B. Deng, Q. Liu, G. Wen, Q. Liu, T. Li, Y. Luo, A. A. Alshehri, K. A. Alzahrani, D. Ma and X. Sun, *Green Chem*., 2021, **23**, 5487–5493.

17 G. Wen, J. Liang, Q. Liu, T. Li, X. An, F. Zhang, A. A. Alshehri, K. A. Alzahrani, Y. Luo, Q. Kong and X. Sun, *Nano Res.*, 2022, **15**, 972–977.

18 G. Wen, J. Liang, L. Zhang, T. Li, Q. Liu, X. An, X. Shi, Y. Liu, S. Gao, A. M. Asiri, Y. Luo, Q. Kong and X. Sun, *J. Colloid Interface Sci*., 2022, **606**, 1055–1063.

19 D. He, Y. Li, H. Ooka, Y. K. Go, F. Jin, S. H. Kim and R. Nakamura, *J. Am. Chem. Soc*., 2018, **140**, 2012–2015.